

Scalar QED, NLO and PHOTOS Monte Carlo.

G. Nanava[†]

*Institute of Nuclear Physics, PAN, Kraków, ul. Radzikowskiego 152, Poland
(On leave from IHEP, TSU, Tbilisi, Georgia)*

and

Z. Wąs

CERN, 1211 Geneva 23, Switzerland

and

Institute of Nuclear Physics, PAN, Kraków, ul. Radzikowskiego 152, Poland

ABSTRACT

Recently, QED bremsstrahlung in B -meson decays into pair of scalars (π 's and/or K 's) is of interest. If experimental acceptance must be taken into account, PHOTOS Monte Carlo is often used in experimental simulations. We will use scalar QED to benchmark PHOTOS, even though this theory is of limited use for complex objects. We present the analytical form of the kernel used in the older versions of PHOTOS, and the new, exact (scalar QED) one. Matrix element and phase-space Jacobians are separated in the final weight and future extensions based on measurable electromagnetic form-factors are thus possible.

The massive phase-space is controlled in the the program with no approximations. Thanks to the iterative solution all leading and next to leading logarithmic terms are properly reproduced by the Monte Carlo simulation. Simultaneously, full differential distributions over complete multiple body phase-space are provided. An agreement of better than 0.01% with independent calculations of scalar QED is demonstrated.

CERN-PH-TH/2006-111,
IFJPAN-IV-2006-5
July, 2006

Supported in part by the EU grant MTKD-CT-2004-510126, in partnership with the CERN Physics Department, and the Polish State Committee for Scientific Research (KBN) grant 2 P03B 091 27 for years 2004-2006.

[†]This work is partly supported by the EU grant mTkd-CT-2004-510126 in partnership with the CERN Physics Department and by the Polish Ministry of Scientific Research and Information Technology grant No 620/E-77/6.PRUE/DIE 188/2005-2008.

1. INTRODUCTION

In the analysis of data from high-energy physics experiments, one tries to resolve the “*experiment = theory*” equation. This non-trivial task requires that a lot of different effects be considered simultaneously. From the experimental side, these are mainly detector acceptance and cuts, which are dictated by the construction and physical properties of the detector. The shapes of distributions may be distorted by, say, misidentification and residual background contamination. These effects need to be discriminated in an appropriate and well-controlled way. From the theoretical side, *all* effects of known physics have to be included in predictions as well. Only then experimental data and theoretical predictions can be confronted to determine numerical values of coupling constants or effects of new physics (to be discovered).

A well-defined class of theoretical effects consists of QED radiative corrections. PHOTOS is a universal Monte Carlo algorithm that simulates the effects of QED radiative corrections in decays of particles and resonances. It is a project with a rather long history: the first version was released in 1991 [1], followed by version 2.0 [2] (double emission and threshold terms for fermions). The package is in wide use [3]; it was applied as a precision simulation tool for the W mass measurement at the Tevatron [4] and LEP [5,6], and for CKM matrix measurements in decays of K and B resonances (NA48 [7], KTeV [8], Belle [9], BaBar [10] and Fermilab [11]). Discussion of the different components of systematic errors in PHOTOS is thus of interest.

Throughout the years the core algorithm for the generation of $O(\alpha)$ corrections did not change much, however, its precision, applicability to various processes, and numerical stability improved significantly. New functionalities, such as multiple photon radiation and interference effects for all possible decays were introduced [12,13]. Recently, the complete first order matrix element was introduced into PHOTOS for Z decays and complete NLO¹ multiple photon predictions for that channel were demonstrated to work well [14].

Increasing interest in the algorithm expressed by experimental collaborations (including future LHC experiments and precise measurements for B decays) was a motivation to perform a more detailed study of the potential and precision of the PHOTOS algorithm. This paper is devoted to the decay of B -mesons into a pair of scalars. It is a continuation of the previous paper [14] devoted to Z decays. We concentrate our attention on exact phase-space parametrization as used in PHOTOS, and on the explicit separation of the final weight into parts responsible for the following: (i) *mass dependent* phase-space Jacobians, (ii) matrix elements and (iii) pre-sampler for peaks.

Simplifications introduced in the matrix element normally used in these scalar B meson decays are removed, the exact kernel of first order scalar QED calculation is installed. Such improvement opens the way to include data dependent form-factors into matrix elements of PHOTOS, and physically better results than of scalar QED alone.

¹In the paper, we will use abbreviations NLO, NLL, NNLO, NNLL to denote next to leading order, next to leading logarithm, next-next to leading order, next-next to leading logarithm corrections with respect to leading order (that is without QED at all). Meaning for such abbreviations can not be defined restrictively on the basis of approximations used in phase-space. The properties of the matrix elements need to be specified as well. Nonetheless, we will use the abbreviations later in the paper to denote such approximations in the phase-space Jacobians which do not prevent the appropriate precision to hold, if proper choice of matrix elements is made as well.

Our study of the PHOTOS algorithm can be understood as another step in the on-going effort to find practical solutions of the improved expansions. The solution can be seen as a rearrangement of the QED perturbation expansion, but this time for the interaction of charged scalars with photons and in the case where ultrarelativistic approximations are not valid.

To test PHOTOS we have used predictions of the SANC [15] Monte Carlo algorithm. SANC is able to calculate the exact first order scalar QED matrix elements for decays of B -mesons into scalars, and covers the full phase space of decay products without any approximations. Events provided by SANC MC are unweighted. SANC is a network client-server system for the semi-automatic calculation of Electroweak, QCD and QED radiative corrections at a one-loop precision level for various processes(-decays) of elementary particle interactions.

The paper is organized as follows. Section 2 is devoted to the description of our results obtained from scalar QED, which will be used later in tests and in construction of kernel for single photon emission. In Section 3 the main properties used in the design of PHOTOS are presented. In particular, the construction of the weight (NLO level) necessary to introduce the complete first order matrix element is explained in all detail. The phase space parametrization used in the iterative solution of PHOTOS is given. Details are collected in the Appendix. On the other hand, quite essential for complete NLL, aspects of the construction will still remain poorly documented. That is, how the parts of the single photon emission matrix element are used in the (iterated and thus extended to the multiphoton emissions) kernel. Section 4 is devoted to results of numerical tests performed at fixed, first order of QED. Some numerical results, obtained with multi-photon version of the program will be collected there for reference. Finally, section 5 summarizes the paper.

2. Scalar QED and B decays

In this section we give the formulae needed in the construction of the Monte Carlo routine of two-particle B -meson decays and the analytical results of the decay rates at $O(\alpha)$ in scalar-QED when the masses of the decay products are neglected. The one-loop QED corrections to the width of the decays $B^{0,-} \rightarrow H_1^- H_2^{+,0}$, where $H_{1,2}$ denotes scalar(pseudo-scalar) particles, can be represented as a sum of the Born contribution and the contributions due to virtual loop diagrams and soft and hard photon emissions. Both virtual and soft contributions factorize to the Born one.

$$d\Gamma^{\text{Total}} = d\Gamma^{\text{Born}} \left[1 + \frac{\alpha}{\pi} \left(\delta^{\text{soft}} + \delta^{\text{virt}} \right) \right] + d\Gamma^{\text{Hard}}. \quad (1)$$

Here $d\Gamma^{\text{Born}}$ is the tree level differential decay width, δ^{virt} represents the virtual corrections, δ^{soft} denotes the soft photon contribution and $d\Gamma^{\text{Hard}}$ is the hard photon contribution. The Born level distribution in the rest frame of the decaying meson can be written as

$$d\Gamma^{\text{Born}} = \frac{1}{2M} |A^{\text{Born}}|^2 dLips_2(P \rightarrow k_1, k_2), \quad (2)$$

where M is the mass of decaying particle, $k_{1,2}$ denote the momenta of decay products, A^{Born} stands for the corresponding tree level amplitude and $dLips_2(P \rightarrow k_1, k_2)$ is the two body differential phase space. For the latter we choose the following parametrization

$$dLips_2(P \rightarrow k_1, k_2) = \frac{1}{32\pi^2} \frac{\lambda^{1/2}(M^2, m_1^2, m_2^2)}{M^2} d\cos\theta_1 d\phi_1, \quad (3)$$

where angles θ_1 and ϕ_1 define the orientation of momentum k_1 in the rest frame of the B -meson. As usual we define $\lambda^{\frac{1}{2}}(a, b, c) = \sqrt{a^2 + b^2 + c^2 - 2ab - 2ac - 2bc}$. In the case of neutral B -meson decay channels $B^0 \rightarrow H_1^- H_2^+$, the scalar-QED calculations for the virtual and soft factors in formula (1) gives

$$\begin{aligned} \delta^{\text{virt}} = & \left[1 + \frac{M^2 - m_1^2 - m_2^2}{\Lambda} \ln \frac{2m_1 m_2}{M^2 - m_1^2 - m_2^2 + \Lambda} \right] \ln \frac{M^2}{m_\gamma^2} + \frac{3}{2} \ln \frac{\mu_{UV}^2}{M^2} \\ & + \frac{M^2 - m_1^2 - m_2^2}{2\Lambda} \left[\text{Li}_2 \left(\frac{M^2 + m_1^2 - m_2^2 + \Lambda}{2\Lambda} \right) - \text{Li}_2 \left(\frac{-M^2 + m_2^2 - m_1^2 + \Lambda}{2\Lambda} \right) \right. \\ & \quad \left. + 2 \ln \frac{2Mm_1}{M^2 + m_1^2 - m_2^2 + \Lambda} \ln \frac{m_1 \Lambda}{M^3} + (1 \leftrightarrow 2) + \pi^2 \right] \\ & - \frac{\Lambda}{2M^2} \ln \frac{2m_1 m_2}{M^2 - m_1^2 - m_2^2 + \Lambda} + \frac{m_2^2 - m_1^2}{4M^2} \ln \frac{m_2^2}{m_1^2} - \frac{1}{2} \ln \frac{m_1 m_2}{M^2} + 1; \end{aligned} \quad (4)$$

$$\begin{aligned} \delta^{\text{soft}} = & \left[1 + \frac{M^2 - m_1^2 - m_2^2}{\Lambda} \ln \frac{2m_1 m_2}{M^2 - m_1^2 - m_2^2 + \Lambda} \right] \ln \frac{m_\gamma^2}{4\omega^2} \\ & + \frac{M^2 - m_1^2 - m_2^2}{2\Lambda} \left[\text{Li}_2 \left(\frac{-2\Lambda}{M^2 + m_1^2 - m_2^2 - \Lambda} \right) - \text{Li}_2 \left(\frac{2\Lambda}{M^2 + m_1^2 - m_2^2 + \Lambda} \right) + (1 \leftrightarrow 2) \right] \\ & - \frac{M^2 + m_1^2 - m_2^2}{\Lambda} \ln \frac{2Mm_1}{M^2 + m_1^2 - m_2^2 + \Lambda} - (1 \leftrightarrow 2), \end{aligned} \quad (5)$$

where $m_{1,2}$ are the final meson masses, an auxiliary small parameter $\omega (\ll M/2)$ separates the soft and hard photon contributions, and μ_{UV} denotes the ultraviolet scale. An auxiliary photon mass m_γ is used as a regulator of the infrared divergences. The ultraviolet singularities are regularized by means of the dimensional regularization. We renormalize the wave functions of the external scalar fields in the on-shell scheme, and the point-like weak coupling in the $\overline{\text{MS}}$ scheme. $\Lambda = \lambda^{1/2}(M^2, m_1^2, m_2^2)$ and $\text{Li}_2(z) = -\int_0^z \frac{dy}{y} \ln|1-y|$.

The hard photon distribution $d\Gamma^{\text{Hard}}$ in scalar-QED can be expressed as follows

$$d\Gamma^{\text{Hard}} = \frac{1}{2M} |A^{\text{Born}}|^2 4\pi\alpha \left(q_1 \frac{k_1 \cdot \varepsilon}{k_1 \cdot k_\gamma} - q_2 \frac{k_2 \cdot \varepsilon}{k_2 \cdot k_\gamma} \right)^2 dLips_3(P \rightarrow k_1, k_2, k_\gamma). \quad (6)$$

Here, $q_{1,2}$ are the charges of final mesons, and k_γ and ε_μ are the photon momentum and polarization vector respectively. The three body differential phase space of the decay products,

$dLips_3(P \rightarrow k_1, k_2, k_\gamma)$, is parametrized, in a rather standard way (see e.g. [16]), as follows:

$$dLips_3(P \rightarrow k_1, k_2, k_\gamma) = \frac{\lambda^{1/2}(1 - 2E_\gamma/M, m_1^2/M^2, m_2^2/M^2)}{16(2\pi)^5 (1 - 2E_\gamma/M)} E_\gamma dE_\gamma d\cos\theta_\gamma d\phi_\gamma d\cos\theta_1^R d\phi_1^R, \quad (7)$$

where the angles θ_1^R and ϕ_1^R define the orientation of momentum k_1 in the rest frame of $(k_1 + k_2)$; the photon energy E_γ and the angles θ_γ and ϕ_γ , that define the orientation of the photon momentum, are given in the rest frame of the decaying particle. These parameters vary in the limits: $0 \leq \theta_\gamma, \theta_1^R \leq \pi$, $0 \leq \phi_\gamma, \phi_1^R \leq 2\pi$ and $\omega \leq E_\gamma \leq (M^2 - (m_1 + m_2)^2)/2M$. The formulae (1)–(7) are used in the construction of the Monte Carlo simulator of the decays under consideration. An analytical integration in (6) over the phase space variables (7) can be done easily. Below we give the result of integration in the massless limit of the final mesons (i.e. $m_1, m_2 \equiv m \rightarrow 0$) because of its simplicity:

$$\Gamma^{\text{Hard}} = \Gamma^{\text{Born}} \frac{\alpha}{\pi} \left[\left(1 - \ln \frac{m^2}{M^2} \right) \ln \frac{4\omega^2}{M^2} - 2 \ln \frac{m^2}{M^2} - \frac{\pi^2}{3} + 4 \right]. \quad (8)$$

The virtual correction depends on the ultraviolet scale μ_{UV} , which should cancel in the total decay width because of the scale dependence of the point-like weak coupling. The infrared divergence cancels out in the sum of virtual and soft contributions, as it must. The total decay width, which is the sum of the contributions (4), (5), and (8), is also free of ω and of the final meson mass singularity in accordance with the KLN theorem [17]–[18]:

$$\Gamma^{\text{Total}} = \Gamma^{\text{Born}} \left[1 + \frac{\alpha}{\pi} \left(\frac{3}{2} \ln \frac{\mu_{UV}^2}{M^2} + 5 \right) \right]. \quad (9)$$

The same calculations can be done for the charged B -meson decay channels $B^- \rightarrow H_1^- H_2^0$. In this case for various contributions in formula (1) we obtain:

– Virtual photon contribution

$$\begin{aligned} \delta^{\text{virt}} = & \left[1 + \frac{M^2 + m_1^2 - m_2^2}{\Lambda} \ln \frac{2Mm_1}{M^2 + m_1^2 - m_2^2 + \Lambda} \right] \ln \frac{Mm_1}{m_\gamma^2} + \frac{3}{2} \ln \frac{\mu_{UV}^2}{Mm_1} \\ & + \frac{M^2 + m_1^2 - m_2^2}{2\Lambda} \left[\text{Li}_2 \left(\frac{M^2 - m_1^2 - m_2^2 + \Lambda}{2\Lambda} \right) - \text{Li}_2 \left(\frac{M^2 - m_1^2 - m_2^2 - \Lambda}{-2\Lambda} \right) \right. \\ & \quad \left. + \text{Li}_2 \left(\frac{M^2 + m_2^2 - m_1^2 - \Lambda}{-2\Lambda} \right) - \text{Li}_2 \left(\frac{M^2 + m_2^2 - m_1^2 + \Lambda}{2\Lambda} \right) \right. \\ & \quad \left. + 2 \ln \frac{2Mm_1}{M^2 + m_1^2 - m_2^2 + \Lambda} \ln \frac{\Lambda}{Mm_2} - \ln \frac{2Mm_2}{M^2 + m_2^2 - m_1^2 + \Lambda} \ln \frac{M^2}{m_1^2} \right] \\ & + \frac{\Lambda}{2m_2^2} \ln \frac{2Mm_1}{M^2 + m_1^2 - m_2^2 + \Lambda} - \frac{M^2 - m_1^2}{4m_2^2} \ln \frac{m_1^2}{M^2} + 1; \end{aligned} \quad (10)$$

– Soft photon contribution

$$\begin{aligned} \delta^{\text{soft}} &= \left[1 + \frac{M^2 + m_1^2 - m_2^2}{\Lambda} \ln \frac{2Mm_1}{M^2 + m_1^2 - m_2^2 + \Lambda} \right] \ln \frac{m_\gamma^2}{4\omega^2} \\ &+ \frac{M^2 + m_1^2 - m_2^2}{2\Lambda} \left[\text{Li}_2 \left(\frac{-2\Lambda}{M^2 + m_1^2 - m_2^2 - \Lambda} \right) - \text{Li}_2 \left(\frac{2\Lambda}{M^2 + m_1^2 - m_2^2 + \Lambda} \right) \right] \\ &- \frac{M^2 + m_1^2 - m_2^2}{2\Lambda} \ln \frac{2Mm_1}{M^2 + m_1^2 - m_2^2 + \Lambda}; \end{aligned} \quad (11)$$

– Hard photon contribution

$$\begin{aligned} d\Gamma^{\text{Hard}} &= \frac{1}{2M} |A^{\text{Born}}|^2 4\pi\alpha \left(q_1 \frac{k_1 \cdot \varepsilon}{k_1 \cdot k_\gamma} - q \frac{P \cdot \varepsilon}{P \cdot k_\gamma} \right)^2 d\text{Lips}_3(P \rightarrow k_1, k_2, k_\gamma), \\ \Gamma^{\text{Hard}} &= \Gamma^{\text{Born}} \frac{\alpha}{\pi} \left[\left(1 + \frac{1}{2} \ln \frac{m^2}{M^2} \right) \ln \frac{4\omega^2}{M^2} + \ln \frac{m^2}{M^2} - \frac{\pi^2}{6} + 3 \right]. \end{aligned} \quad (12)$$

Again after integration over the phase space variables, the massless limit of the final mesons (i.e. $m_1, m_2 \equiv m \rightarrow 0$) was used in the last formula. Finally, summing contributions (10), (11) and (12), we obtain the following expression for the total decay width:

$$\Gamma^{\text{Total}} = \Gamma^{\text{Born}} \left[1 + \frac{\alpha}{\pi} \left(\frac{3}{2} \ln \frac{\mu_{UV}^2}{M^2} - \frac{\pi^2}{3} + \frac{11}{2} \right) \right]. \quad (13)$$

We have checked that the factors δ^{soft} and δ^{virt} in formula (1), for both charged and neutral B -meson decays, provide the same numerical results as the corresponding expressions in [19].

To be assured of the accuracy of SANC Monte Carlo integration (which is a by-product of MC simulation), we compared Monte Carlo results with the analytical calculations of the total decay rate. The result of this comparison is shown in Table 1². The agreement is thus better than 10^{-4} in this test, where mass effects were included.

Channel	$\Gamma_{\text{AC}}^{\text{Total}}, 10^{-3}\text{MeV}$	$\Gamma_{\text{MC}}^{\text{Total}}, 10^{-3}\text{MeV}$
$B^- \rightarrow \pi^- \pi^0$	0.373629	0.3736(4)
$B^- \rightarrow K^- K^0$	0.367586	0.3675(9)
$B^0 \rightarrow \pi^- \pi^+$	0.377392	0.3773(8)
$B^0 \rightarrow K^- K^+$	0.371414	0.3714(2)

Table 1: Comparison of the B -meson total decay widths produced by analytical calculations (second column) and by Monte Carlo (third column). The last significant digit of the Monte Carlo results is given in bracket.

²Please note that these numbers are for the purpose of our test only, the overall $B-H-H$ coupling constants do not match the experimental data.

3. Exact phase-space and matrix element.

To start any discussion of the implementation of complete first order QED radiative corrections in B decay, one has to specify the parametrization of the complete phase-space slots of the fixed final state multiplicity.

Let us start with the explicit expression for the parametrization of an $n + 1$ body phase-space in decay of the object of four-momentum P ($P^2 = M^2$), as used in PHOTOS Monte Carlo. As our aim is to define iterative relations, let us denote the four momenta of the first n decay products as k_i ($i = 1, n$) and the last $n + 1$ decay product as k_{n+1} . In our case the $n + 1$ -th particle will always be the real and massless photon³. In the later steps of our construction the masslessness of photons and properties of QED matrix elements will be used.

In the following, notation from refs. [20,21] will be used. We will not rely on any particular results of these papers. We only point to other, similar options for the exact n -body phase-space parametrizations, which are also in use.

The Lorentz invariant phase-space is defined as follows:

$$\begin{aligned}
dLips_{n+1}(P) &= \frac{d^3 k_1}{2k_1^0 (2\pi)^3} \cdots \frac{d^3 k_n}{2k_n^0 (2\pi)^3} \frac{d^3 k_{n+1}}{2k_{n+1}^0 (2\pi)^3} (2\pi)^4 \delta^4 \left(P - k_{n+1} - \sum_{i=1}^n k_i \right) \\
&= d^4 p \delta^4 (P - p - k_{n+1}) \frac{d^3 k_{n+1}}{2k_{n+1}^0 (2\pi)^3} \frac{d^3 k_1}{2k_1^0 (2\pi)^3} \cdots \frac{d^3 k_n}{2k_n^0 (2\pi)^3} (2\pi)^4 \delta^4 \left(p - \sum_{i=1}^n k_i \right) \\
&= d^4 p \delta^4 (P - p - k_{n+1}) \frac{d^3 k_{n+1}}{2k_{n+1}^0 (2\pi)^3} dLips_n(p \rightarrow k_1 \dots k_n), \tag{14}
\end{aligned}$$

where extra integration variables, four vector p (compensated with $\delta^4(p - \sum_1^n k_i)$) is introduced. If further, $M_{1\dots n}$ (compensated with $\delta(p^2 - M_{1\dots n}^2)$) is introduced, the element of the phase space takes the form:

$$\begin{aligned}
dLips_{n+1}(P) &= \frac{dM_{1\dots n}^2}{(2\pi)} dLips_2(P \rightarrow p k_{n+1}) \times dLips_n(p \rightarrow k_1 \dots k_n) \\
&= dM_{1\dots n}^2 \left[d \cos \hat{\theta} d\hat{\phi} \frac{1}{8(2\pi)^3} \frac{\lambda^{\frac{1}{2}}(M^2, M_{1\dots n}^2, m_{n+1}^2)}{M^2} \right] \times dLips_n(p \rightarrow k_1 \dots k_n). \tag{15}
\end{aligned}$$

The part of the phase space Jacobian corresponding to integration over the direction and energy of the last particle (or equivalently invariant mass $M_{1\dots n}$ of the remaining system of $1\dots n$ particles) is explicitly given. We will use later in the formulas $m_i^2 = k_i^2$, and analogously $M_{i\dots n}$, defining invariant masses of $k_i \dots k_n$ systems. The integration over the angles $\hat{\theta}$ and $\hat{\phi}$ is defined in the P rest-frame. The integration over the invariant mass, $M_{1\dots n}$, is limited by phase space

³However the construction does not rely on a photon to be massless. In principle it can be applied to define other phase space relations, for example the emission of an extra massive pion or emission of a pair of heavy particles.

boundaries. Anybody familiar with the phase-space parametrization as used in FOWL [16], TAUOLA [21], or many other programs will find the above explanation quite standard⁴.

The question of choice of axes with respect to which angles are defined, and order in kinematical construction, is less trivial. The choice for the particular option stems from necessity to presample collinear singularities. It is rather well known that the choice of the reference directions for the parametrization of the unit sphere is free, and can be used to advantage. We will use related, but somewhat different freedom of choice. Instead of variables $\hat{\theta} \hat{\phi}$ defining orientation of k_{n+1} in P rest-frame we will use angles $\theta_1 \phi_1$ orienting k_1 (also in P rest-frame). The Jacobian for this reparametrization of unit sphere equals 1 as well⁵.

Formula (15) can be iterated and provide a parametrization of the phase space with an arbitrary number of final state particles. In such a case, the question of orientation of the frames used to define the angles and the order of $M_{i\dots n}$ integrations (consequently, the choice of limits for $M_{i\dots n}$ integration), becomes particularly rich. Our choice is defined in ref. [2]. We will not elaborate on this point here, nothing new was introduced for the purpose of our study.

If the invariant mass $M_{1\dots n}$ is replaced with the photon energy defined in the P rest-frame, k_γ , then the phase space formula can be written as:

$$dLips_{n+1}(P) = \left[k_\gamma dk_\gamma d \cos \hat{\theta} d\hat{\phi} \frac{1}{2(2\pi)^3} \right] \times dLips_n(p \rightarrow k_1 \dots k_n), \quad (16)$$

If we would have l photons accompanying n other particles, then the factor in square brackets is iterated. The statistical factor $\frac{1}{l!}$ would complete the form of the phase space parametrization, similar to the formal expansion of the exponent. The last formula, supplemented with definition of frames with respect to which angles are defined is used to define the full kinematic configuration of the event. From angles and energies (k_{γ_i}) of photons and also angles, energies and masses for other decay products, four-momenta of all final state particles can be constructed.

If in formula (16) instead of $dLips_n(p \rightarrow k_1 \dots k_n)$ one would use $dLips_n(P \rightarrow k_1 \dots k_n)$ the **tangent space** would be obtained. Then k_{n+1} photon does not affect other particles' momenta at all, and thus has no boundaries on energy or direction. If this formula would be iterated then all such photons would be independent from one another as well⁶. Energy and momentum constraints on the photon(s) are introduced with the relation between tangent and real $n + 1$ -

⁴The parametrizations of such a type, use properties of the Lorentz group in an explicit manner, in particular measure, representations and their products. That is why, they are useful, for event building Monte Carlo programs in phase-space constructions based on boosts and rotations.

⁵Let us point to another difference with respect to angles θ_1^R, ϕ_1^R used in formula (7) (and also in refs. [16], [21]). For example, if $n = 2$ then our $dLips_{n=2}$ phase-space is parametrized by the angles θ and ϕ only. The two angles will define orientation of k_γ with respect to frame used for quantization of internal state of k_1 , this is different choice than the one used for ϕ_1^R , even though $\theta = \theta_1^R$. The Jacobian for the corresponding change of variables equals 1 also.

⁶Expression (16) would be slightly more complicated if instead of photons a massive particle was to be added.

body phase-space. The formula defining one step in the iteration reads as follows⁷:

$$\begin{aligned}
dLips_{n+1}(P \rightarrow k_1 \dots k_n, k_{n+1}) &= dLips_n^{+1 \text{ tangent}} \times W_n^{n+1}, \\
dLips_n^{+1 \text{ tangent}} &= dk_\gamma d \cos \theta d\phi \times dLips_n(P \rightarrow \bar{k}_1 \dots \bar{k}_n), \\
\{k_1, \dots, k_{n+1}\} &= \mathbf{T}(k_\gamma, \theta, \phi, \{\bar{k}_1, \dots, \bar{k}_n\}).
\end{aligned} \tag{17}$$

The W_n^{n+1} depends on details of \mathbf{T} , and will be thus given later in formula (23). To justify (17), we have to convolute formula (15) for $Lips_{n+1}(P \rightarrow k_1 \dots k_n, k_{n+1})$ with itself (for $Lips_n(p \rightarrow k_1 \dots k_n)$):

$$\begin{aligned}
Lips_{n+1}(P \rightarrow k_1 \dots k_n, k_{n+1}) &= \frac{dM_{1\dots n}^2}{2\pi} Lips_2(P \rightarrow k_{n+1} p) \times Lips_n(p \rightarrow k_1 \dots k_n) \\
Lips_n(p \rightarrow k_1 \dots k_n) &= \frac{dM_{2\dots n}^2}{2\pi} Lips_2(p \rightarrow k_1 p') \times Lips_{n-1}(p' \rightarrow k_2 \dots k_n)
\end{aligned} \tag{18}$$

and use it also for $Lips_n(P \rightarrow \bar{k}_1 \dots \bar{k}_n)$:

$$Lips_n(P \rightarrow \bar{k}_1 \dots \bar{k}_n) = \frac{dM_{2\dots n}^2}{2\pi} Lips_2(P \rightarrow \bar{k}_1 \bar{p}') \times Lips_{n-1}(\bar{p}' \rightarrow \bar{k}_2 \dots \bar{k}_n). \tag{19}$$

Note that our tangent space of variables $dk_\gamma d \cos \theta d\phi$ is unbounded from above and the limit is introduced by W_n^{n+1} which is set to zero for the configurations outside the phase-space. In principle, we should distinguish between variables like $M_{2\dots n}$ for invariant mass of $k_2 \dots k_n$ and $\bar{M}_{2\dots n}$ for invariant mass of $\bar{k}_2 \dots \bar{k}_n$, but in our choice for G_n, G_{n+1} below, $M_{2\dots n} = \bar{M}_{2\dots n}$ and $M_{1\dots n}$ is defined anyway for the $n+1$ -body phase space only.

We direct the reader to refs. [1, 2] for an alternative presentation. Let us remark that formula (17) is quite general, many options, motivated by the properties of the matrix elements, can be introduced. Generally the transformation T may differ from the choice to choice quite a lot. The most straightforward choice can be based on any n and $n+1$ body phase-space parametrizations using invariant masses and angles (e.g. exactly as in TAUOLA [21] formulas 11 to 13).

If

$$G_n : M_{2\dots n}^2, \theta_1, \phi_1, M_{3\dots n}^2, \theta_2, \phi_2, \dots, \theta_{n-1}, \phi_{n-1} \rightarrow \bar{k}_1 \dots \bar{k}_n \tag{20}$$

and

$$G_{n+1} : k_\gamma, \theta, \phi, M_{2\dots n}^2, \theta_1, \phi_1, M_{3\dots n}^2, \theta_2, \phi_2, \dots, \theta_{n-1}, \phi_{n-1} \rightarrow k_1 \dots k_n, k_{n+1} \tag{21}$$

then

$$\mathbf{T} = G_{n+1}(k_\gamma, \theta, \phi, G_n^{-1}(\bar{k}_1, \dots, \bar{k}_n)). \tag{22}$$

The ratio of the Jacobians (factors $\lambda^{1/2}$ like in formula (15), etc.) form the factor W_n^{n+1} , which in our case is rather simple,

$$W_n^{n+1} = k_\gamma \frac{1}{2(2\pi)^3} \times \frac{\lambda^{1/2}(1, m_1^2/M_{1\dots n}^2, M_{2\dots n}^2/M_{1\dots n}^2)}{\lambda^{1/2}(1, m_1^2/M^2, M_{2\dots n}^2/M^2)}, \tag{23}$$

⁷The $\{\bar{k}_1, \dots, \bar{k}_n\}$ can be identified with the event before the radiation of k_γ is introduced.

because of choice for G as explained in the Appendix. Note that $k_\gamma = \frac{M^2 - M_{1\dots n}^2}{2M}$. There are additional benefits from such a choice. In all relations $\bar{k}_2 = Lk_2, \dots, \bar{k}_n = Lk_n$ and $\bar{p}' = Lp'$ common Lorentz transformation L is used. Transformation L is defined from $k_1, \bar{k}_1, \bar{p}', p'$ and P ; internal relations between four vectors $k_2 \dots k_n, (\bar{k}_2 \dots \bar{k}_n)$ are not needed.

Formula (17) can be realized algorithmically in the following way:

1. For any point in n -body phase space (earlier generated event), described for example with the explicit configuration of four vectors $\bar{k}_1 \dots \bar{k}_n$, coordinate variables can be calculated, using formula (20).
2. Photon variables can be generated according to Eq. (17). The weight W_n^{n+1} has to be also attributed.
3. Variables obtained in this way from the old configuration and the one of a photon can be used to construct the new kinematical configuration for the $n + 1$ -body final state. The phase-space weight, which is zero for configurations outside phase space boundaries, can be calculated at this point from (17,23) and finally combined with the matrix element.

Here we have chosen two sub-groups of particles. The first one consisted of particle 1 alone, and the second, of particles 2 to n combined together. Obviously in the case of 2-body decays as discussed in this paper, there is not much choice when construction of the first photon is performed.

By iteration, we can generalize formula (17) to the case of l photons and we write:

$$dLips_{n+l}(P \rightarrow k_1 \dots k_n, k_{n+1} \dots k_{n+l}) = \frac{1}{l!} \prod_{i=1}^l \left[dk_{\gamma_i} d \cos \theta_{\gamma_i} d\phi_{\gamma_i} W_{n+i-1}^{n+i} \right] \times dLips_n(P \rightarrow \bar{k}_1 \dots \bar{k}_n),$$

$$\{k_1, \dots, k_{n+l}\} = \mathbf{T}(k_{\gamma_l}, \theta_{\gamma_l}, \phi_{\gamma_l}, \mathbf{T}(\dots, \mathbf{T}(k_{\gamma_1}, \theta_{\gamma_1}, \phi_{\gamma_1}, \{\bar{k}_1, \dots, \bar{k}_n\}) \dots)). \quad (24)$$

In this formula we can easily localize the **tangent space** for the multiple photon configuration. In this space, each photon is independent from other particles' momenta. Note that it is also possible to fix upper boundary on k_{γ_i} arbitrary high. Photons are independent one from another as well. Correlations appear later, thanks to iterated transformation \mathbf{T} . The factors W_{n+i-1}^{n+i} are calculated when constraints on each consecutive photon are introduced; the previously constructed ones are included in the $n + i - 1$ system⁸.

Of course, for the tangent space to be useful, the choice of the definition of \mathbf{T} must be restricted at least by the condition $\{k_1, \dots, k_n\} \rightarrow \{\bar{k}_1, \dots, \bar{k}_n\}$ if all $k_{\gamma_i} \rightarrow 0$.⁹

It is important to realize that one has to choose matrix elements on the tangent space to complete the construction used in PHOTOS. The number and energies of photons will be generated on the tangent space first. Regularization of (at least) soft singularity must be defined.

⁸Configurations of k_{γ_i} which can not be resolved are replaced with the ones of that photon dropped out.

⁹In fact further constraints have to be fulfilled to enable presampling for the collinear singularities. Note that variables $k_{\gamma_m}, \theta_{\gamma_m}, \phi_{\gamma_m}$ are used at a time of the m -th step of iteration only, and are not needed elsewhere in construction of the physical phase space; the same is true for invariants and angles $M_{2\dots n}^2, \theta_1, \phi_1, \dots, \theta_{n-1}, \phi_{n-1} \rightarrow \bar{k}_1 \dots \bar{k}_n$ of (20,21), which are also redefined at each step of the iteration.

Rejection, and event construction, is performed with the help of formula (17) for each consecutive photon. It diminishes photon multiplicity with respect to the one defined for the tangent space. Of course, as rejection implements changes in phase-space density, a matrix element (with virtual corrections) of the physical space can be introduced as well.

The treatment of the phase space presented here lies at the heart of the construction of PHOTOS kinematics, and was used since its beginning. It exhausts the case when there is only one charged particle in final state. For multiple charged particle final states new complication appear, because all collinear configurations need simultaneous attention, and not only the one along k_1 direction. A presampler with multichannel generation is needed. In our case we follow the same method¹⁰ as explained in ref. [21].

In the standard version of PHOTOS, as published in [1, 2], the following matrix element is used for single photon emission when there is *only one charged particle* in final state:

$$|\mathcal{M}|_{PHOTOS}^2 = |A^{B\text{orn}}|^2 WT_3^{old} \quad (25)$$

where

$$\begin{aligned} WT_3^{old} &= \frac{4\pi\alpha}{WT_1 WT_2} \frac{2(1-x)}{1+(1-x)^2} \left(1 - \frac{m_R^2}{1-\beta^2 \cos^2 \theta}\right) \frac{1+\beta \cos \theta}{2} \frac{1-\sqrt{1-m_R^2} \cos \theta}{1-\beta \cos \theta} \\ \beta &= \sqrt{1 - 4 \frac{m_1^2}{M^2(1-x)} \frac{1}{(1-x + (m_1^2 - m_2^2)/M^2)^2}} \\ x &= \frac{2E_\gamma}{M} \frac{M^2}{M^2 - (m_1 + m_2)^2}, \quad m_R^2 = 4 \frac{m_1^2}{M^2(1 + m_1^2/M^2)^2}. \end{aligned} \quad (26)$$

The old and lengthy approximation WT_3^{old} for WT_3 implemented in standard PHOTOS is kept for compatibility with ref. [2]. The expression defining WT_3 without approximations reads:

$$\begin{aligned} |\mathcal{M}|_{exact}^2 &= |A^{B\text{orn}}|^2 4\pi\alpha \left(q_1 \frac{k_1 \cdot \varepsilon}{k_1 \cdot k_\gamma} - q \frac{P \cdot \varepsilon}{P \cdot k_\gamma} \right)^2 \\ &= |A^{B\text{orn}}|^2 4\pi\alpha \frac{8}{M^2} \times \frac{\lambda \left(1, \frac{m_1^2}{\tau}, \frac{m_2^2}{\tau}\right) \left(1 - \frac{2E_\gamma}{M}\right) \sin^2 \theta}{2 \left(\frac{2E_\gamma}{M}\right)^2 \left(1 + \frac{m_1^2 - m_2^2}{\tau} - \lambda^{1/2} \left(1, \frac{m_1^2}{\tau}, \frac{m_2^2}{\tau}\right) \cos \theta\right)^2} \\ &= |A^{B\text{orn}}|^2 4\pi\alpha \frac{8}{M^2} \times WT_3(P, k_1, k_2, k_\gamma); \end{aligned} \quad (27)$$

here, $(k_1 + k_2)^2 = \tau$. In both, the standard and exact version of PHOTOS, the same phase-space parametrization and presampler for collinear and soft singularities are used. Together with WT_3 the following factors related to phase space WT_1 , WT_2 , contribute to the final weight

¹⁰We will omit details here, because for the two-body final states the complications manifest themselves only in the case of multiple photon generation, see Appendix.

implemented in routine PHOCOR of PHOTOS:

$$\begin{aligned}
WT_1(P, k_1, k_2, k_\gamma) &= \frac{\lambda^{1/2} \left(1, \frac{m_1^2}{M^2}, \frac{m_2^2}{M^2}\right) 2E_\gamma}{\lambda^{1/2} \left(1, \frac{m_1^2}{\tau}, \frac{m_2^2}{\tau}\right) M} \\
WT_2(P, k_1, k_2, k_\gamma) &= \frac{2(1 - \cos\theta \sqrt{1 - m_R^2}) M}{1 + (1 - x)^2} \frac{M}{2E_\gamma}
\end{aligned} \tag{28}$$

The expression for WT_1 can be deciphered from formula (17) and WT_2 is related to presamplers for collinear and soft singularities. The factors WT_1 and WT_2 are used in present paper in definition of WT_3^{old} (formula 26) only.

The combined effect of the virtual and real corrections on the total rate manifests through $\frac{\Gamma^{\text{Total}}}{\Gamma^{\text{Born}}}$. The virtual corrections are included into PHOTOS through this factor. Let us point that the ratio of (27) and (25) constitutes the basic element of upgrading PHOTOS functionality to the complete first order¹¹. The correcting weight can be chosen simply as:

$$wt = \frac{|\mathcal{M}|_{\text{exact}}^2 \Gamma^{\text{Born}}}{|\mathcal{M}|_{\text{PHOTOS}}^2 \Gamma^{\text{Total}}}. \tag{29}$$

For the standard version of PHOTOS the virtual corrections are required to be such that the total decay rate remains unchanged after complete QED corrections are included.

In case of final states with two charged particles in PHOTOS the formula (29) need to be modified with one of the following versions of the interference weight:

$$\begin{aligned}
wt &= \sum_{i=1,2} \frac{|\mathcal{M}|_{\text{exact}}^2}{|\mathcal{M}|_{\text{PHOTOS}}^2} \Big|_i \frac{\Gamma^{\text{Born}}}{\Gamma^{\text{Total}}} WT_{\text{INT}}^i \\
WT_{\text{INT}}^i &= \frac{\left(q_1 \frac{k_1 \cdot \varepsilon}{k_1 \cdot k_\gamma} - q_2 \frac{k_2 \cdot \varepsilon}{k_2 \cdot k_\gamma}\right)^2}{\left(q_1 \frac{k_1 \cdot \varepsilon}{k_1 \cdot k_\gamma} - q_1 \frac{P \cdot \varepsilon}{P \cdot k_\gamma}\right)^2 + \left(q_2 \frac{k_2 \cdot \varepsilon}{k_2 \cdot k_\gamma} - q_2 \frac{P \cdot \varepsilon}{P \cdot k_\gamma}\right)^2} \\
WT_{\text{INT-option}}^i &= J_i \frac{\left(q_1 \frac{k_1 \cdot \varepsilon}{k_1 \cdot k_\gamma} - q_2 \frac{k_2 \cdot \varepsilon}{k_2 \cdot k_\gamma}\right)^2}{\left(q_1 \frac{k_1 \cdot \varepsilon}{k_1 \cdot k_\gamma} - q_1 \frac{P \cdot \varepsilon}{P \cdot k_\gamma}\right)^2 J_1 + \left(q_2 \frac{k_2 \cdot \varepsilon}{k_2 \cdot k_\gamma} - q_2 \frac{P \cdot \varepsilon}{P \cdot k_\gamma}\right)^2 J_2} \\
J_1 &= \frac{1}{WT_1(P, k_1, k_2, k_\gamma) WT_2(P, k_1, k_2, k_\gamma)} \\
J_2 &= \frac{1}{WT_1(P, k_2, k_1, k_\gamma) WT_2(P, k_2, k_1, k_\gamma)}
\end{aligned} \tag{30}$$

The sum over two generation channels $i = 1, 2$ related to emission from q_1 and q_2 is to be performed¹². The form of WT_{INT}^i results from the exact expressions, formulae (12) and (6).

¹¹ When the option of multiple radiation is used in PHOTOS, the single photon emission kernel is iterated. This leads to some complications.

¹²Formulae (27) and (25) for $|\mathcal{M}|_{\text{exact}}^2$ and $|\mathcal{M}|_{\text{PHOTOS}}^2$ are for emissions in case of single charge final state only, the interference weight is to introduce the exact matrix element for process of two charged scalar final state.

However, phase space and multichannel presampler specific terms (28) need to be discussed. Presence of J_1 and J_2 in interference weight is optional, but only for single photon radiation. The factor $J_{1,2}$ (J_1 or J_2) should cancel the $WT_1 \cdot WT_2$ term of the generation branch used for this particular event generation. In general, the absence of $J_{1,2}$ terms is due to properties of the second order matrix element¹³. For the time being analogies to the case of Z decay have to be used instead of the proof.

Once we have completed the description of our internal correcting weight necessary for PHOTOS to work in the NLO regime, we will turn to the numerical results.

4. Results of the tests

The most attractive property of Monte Carlo is the possibility to implement selection criteria for the theoretical predictions that coincide with the experimental ones. Especially in the case of the final state bremsstrahlung presence of experimental cut-offs is essential, as they usually significantly increase the size of the QED effects.

In this section we will concentrate however, on the following pseudo-observables, as used in ref. [22, 23]:

- *Photon energy in the decaying particle rest frame*: this observable is sensitive mainly to the leading-log (i.e. collinear) non-infrared (i.e. not soft) component of the distributions.
- *Energy of the final-state charged particle*: as the previous one, this observable is sensitive mainly to the leading-log (i.e. collinear) non-infrared (i.e. not soft) component of the distributions.
- *Angle of the photon with final-state charged particle*: this observable is sensitive mainly to the non-collinear (i.e. non-leading-log) but soft (i.e. infrared) component of the distributions.
- *Acollinearity angle of the final-state scalars*: this observable is sensitive mainly to the non-collinear (i.e. non-leading-log) and non-soft (i.e. non-infrared) component of the distributions.

We will start our comparison for $B^- \rightarrow \pi^0 K^- (\gamma)$ and PHOTOS running without improvements from the complete matrix element: the agreement looks good, see fig. 1, and holds over the entire range of the distributions, even though densities vary by up to 8 orders of magnitude. Differences can hardly be seen. To visualize the differences, in fig. 2, the ratios of the distributions are plotted. Similar to what was seen in the tests for Z decays [14] local discrepancies may reach up to 15 % for $\cos \theta_{acoll.} > 0.5$. Note however that those regions of the phase-space contribute at the level of 10^{-6} to the total decay rate. Once the matrix element is switched on, see fig. 3, where ratios of distribution are plotted, the agreement become excellent, even at a

¹³For example the form $WT_{INT-option}$ is inappropriate for configurations when the first generated photon is hard and the second soft.

statistical level of 10^9 events. It was of no use to repeat the plots of the distributions with the corrected weight in PHOTOS, as the plots could not be distinguished from the ones of fig. 1.

Encouraged by the excellent performance in the case of the decay into final states with a single charged particle, let us now turn to decays into two charged mesons. To avoid accidental simplifications, we have selected final states with scalars of different masses ($B^0 \rightarrow \pi^- K^+(\gamma)$).

Again, as can be seen from figs. 4 and 5, agreement between PHOTOS using the standard kernel and SANC is rather good, but some differences persist. Once the complete kernel is switched on, fig. 6, the agreement is quite amazing. In this case, the interference weight, and the multiple singularity structure of the pre-sampler Jacobians, formula (30), were tested as well. Both versions WT_{INT} and $WT_{INT-option}$ gave the same results for the case of single photon emission. However only the first version, WT_{INT} turned out to be consistent with exponentiation. To complete the tests for multichannel emissions, final states with more than two massive decay products need to be studied, preferably for multi-photon radiation as well.

Let us comment that not only the shapes of the distribution agree in an excellent manner between PHOTOS and SANC simulations, also the number of events with photons of energy below the certain threshold agreed better than 0.01 %, thus were consistent with each other within a statistical error of 10^9 event samples. The excellent agreement, presented in our paper, combined with other results published before, help to confirm that theoretical effects normally missing in PHOTOS are small, but if necessary can be introduced into the code. It is also important to note that the agreement provides powerful technical test of the generator.

Finally, let us point out that early versions of the program, before 2004, were not reaching that level of technical sophistication. To establish it required a major effort. Kinematical variables used in PHOTOS differ from those of SANC. The differences could arise due to technical problems, also if for example the Born-level events which are to be modified by PHOTOS would not fulfill energy-momentum conservation or particles momenta were not on mass-shell, at the numerical double precision level. This point must always be checked for every new installation of PHOTOS in an experimental environment. For that purpose we have collected numerical results, given in Table 2., for the cumulant of bremsstrahlung decay width: $G(E_{test}) = \Gamma(E_{test})/\Gamma^{Total}$, where $\Gamma(E_{test})$ denotes the decay width, integrated over energy carried by all bremsstrahlung photons combined up to maximum of E_{test} .

5. Summary

This paper was devoted to the study of bremsstrahlung corrections in the decay of B -mesons into pair of scalars of rather large masses. The results were presented in the analytical form and Monte Carlo simulations which were later compared.

To quantify the size of the Next to Leading order effects normally missing in PHOTOS we have installed into the program the complete scalar-QED first order expression for the B decay matrix element. After modification, the differences between PHOTOS and the matrix element calculation embodied in SANC were below statistical error of 10^9 events for all of our benchmark distributions. Both PHOTOS and SANC were run at fixed first order without

exponentiation. The agreement provides a technical test of the simulations from both of the two programs as well.

The improvement of the agreement due to the introduction of a correcting weight could come with a price. That was the case with the decay of Z . However because our B -mesons are scalar, the complications did not materialize and a correcting weight can be installed to standard PHOTOS versions. On the other hand, introduced improvements are numerically small. Deficiencies of standard PHOTOS are localized in corners of bremsstrahlung phase space populated by photons of very high energies and angularly well separated from final state mesons. Those regions of the phase space weigh less than 0.005 to the total rate and differences in that region approach 20 % of their size, at most. The effects are thus significantly lower than 0.1 %, if quantified in units of the integrated B decay rate of a particular channel. Also, in those regions, the predictive power of scalar QED is rather doubtful. That is why we do not think it is urgent for users to change the PHOTOS correcting weight to enable the complete NLO, unless measured form-factors become available. Contribution to the systematic error of PHOTOS due to incompleteness of the old kernel (with respect to scalar QED) does not depend on experimental cuts and is thus of no phenomenological importance for today.

Our paper was not only focused on numerical results due to final state bremsstrahlung in B decays. Aspects of mathematical organization of the program for calculation of radiative corrections for B production and decay was discussed as well. Approximations used in PHOTOS affects matrix elements and *not* phase space, which is treated exactly including all mass effects.

Details of phase-space parametrization and other aspects necessary for implementation of NLO effects are collected for the first time. Generation of the phase space starts from the tangent space constructed from an eikonal approximation but used also for the hard photons, even of energies above the available maximum. In the second step, phase-space constraints are enforced. The method is similar to exclusive exponentiation [24].

Complete re-analysis of the final weight for decays into scalars was presented. Parts corresponding to matrix elements, phase space Jacobians and generator pre-samples were explicitly separated. Special care was devoted to mass terms. Analytic form of the single photon emission kernel (i. e. matrix element with approximation) used in standard version of PHOTOS, was also explicitly given. That is why, the analysis presented here can be easily extended to other decay channels. It is the first time that we have presented such a study for particles other than elementary fermions and in the case where mass terms of order $\frac{\alpha}{\pi} \frac{m_{1,2}^2}{M^2}$ are not neglected. Our analytical calculations agree with the results of reference [19] exactly and could serve as a basis of our technical tests of the program.

The numerical results collected in Table 2. can be used as a technical test of PHOTOS installation in end-user simulation set-ups. We strongly recommend such tests to be performed. In these tests the agreement between PHOTOS and SANC (or simple semi-analytical expressions for higher order simulations) was significantly better than 0.1 % for all entries.

In case of program operating for multiple photon radiation, energy momentum constraints are introduced for each consecutive photon, step by step, and conformal symmetry is not exploited in that procedure. Details of phase-space parametrization used for multiple photon radiations were presented. In principle, for B decays and multiple photon radiation in PHO-

TOS, a similar level of agreement as in ref. [14] for Z decay is expected, but the appropriate reference distributions do not exist yet. In particular the second order, scalar-QED, matrix element for B decays was not available for us. That is why we think, that the matrix-element related details of the program construction, necessary for implementation of NLL effects in general case, must remain delegated to the forthcoming work; probably to the times, when we will have at our disposal other second order matrix elements than just of $Z \rightarrow l\bar{l}$. At present, only dispersed (and for NLL based on analogies with Z decays only) results of refs. [2, 14, 25] are available for that purpose.

PHOTOS used for decays of B -mesons into scalars provides an example of program working for multiple emissions from both outgoing charged lines. It covers complete phase space, no special treatment is needed for the hard photon emission regions. Also mass terms have been included without any approximations.

On the technical level it is worth mentioning that the NLO correcting weight of PHOTOS is used as an internal weight. All generated events remain weight 1, exactly as it was in the case of $Z \rightarrow \mu^+\mu^-$ decay.

In principle, if necessary, even complete higher order matrix elements (NNLO level) could be incorporated with the help of correcting weights. This interesting point definitely goes beyond the scope of the present paper and also beyond the phenomenological interest for any foreseeable future. This is equally true for the possible extensions to simulations in QCD, which are also outside the scope of the paper.

Acknowledgements.

Useful discussions with E. Barberio, P. Golonka, Z. Nagy, F. Tkachov and T. Sjöstrand are acknowledged.

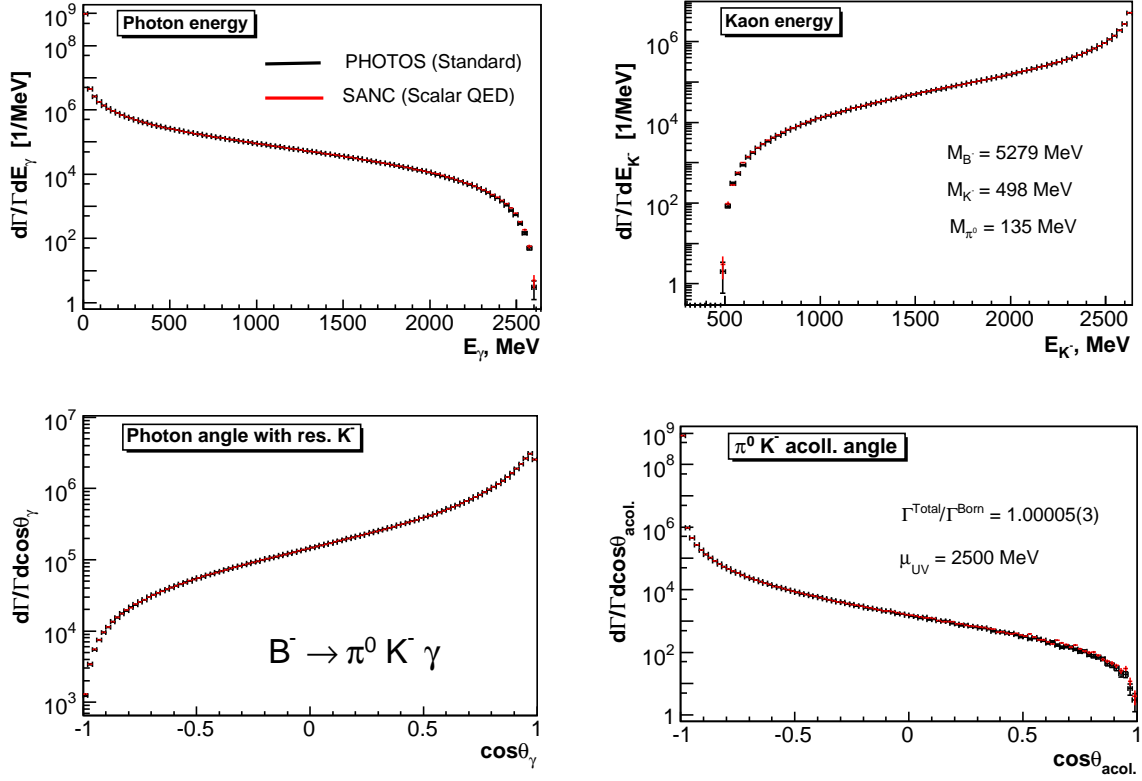


Figure 1: Results from PHOTOS, standard version, and SANC for $B^- \rightarrow \pi^0 K^- (\gamma)$ decay are superimposed on the consecutive plots. Standard distributions, as defined in the text, and logarithmic scales are used. The distributions from the two programs overlap almost completely. Samples of 10^9 events were used. The ultraviolet scale, μ_{UV} , was chosen to leave total decay width unchanged by QED.

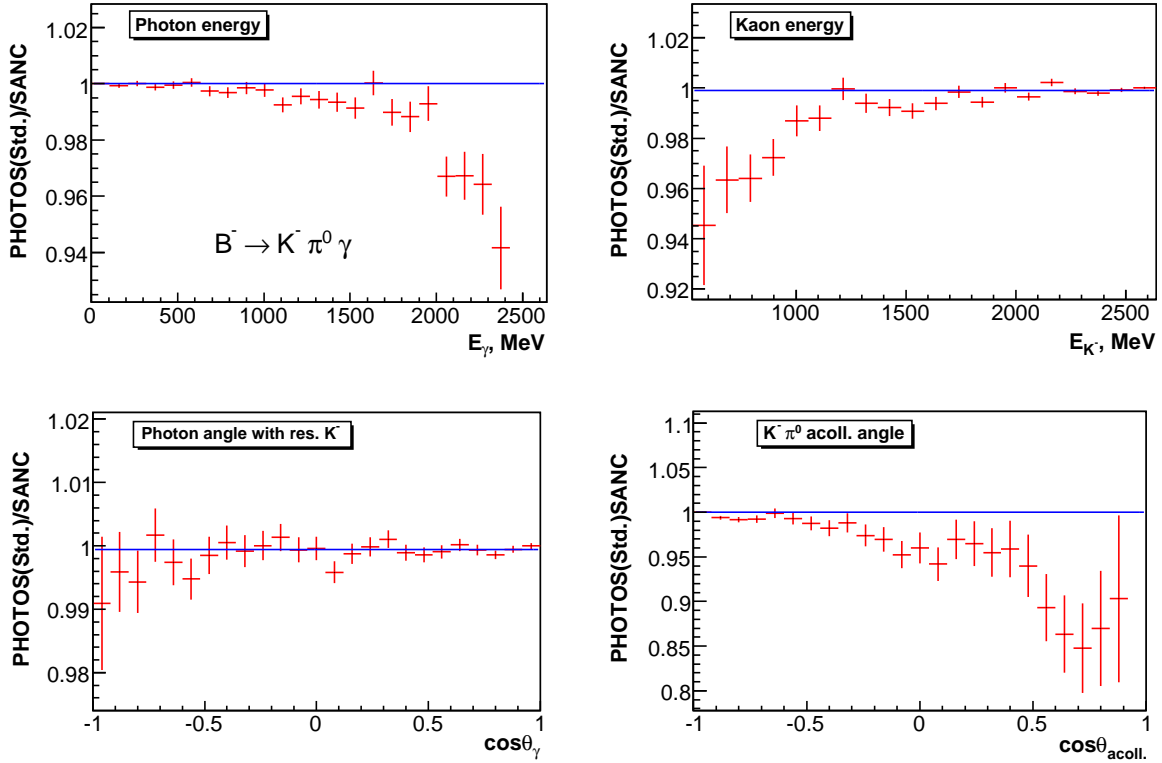


Figure 2: Results from PHOTOS, standard version, and SANC for ratios of the $B^- \rightarrow \pi^0 K^- (\gamma)$ distribution in fig.1 are presented. Differences between PHOTOS and SANC are small, but are clearly visible now.

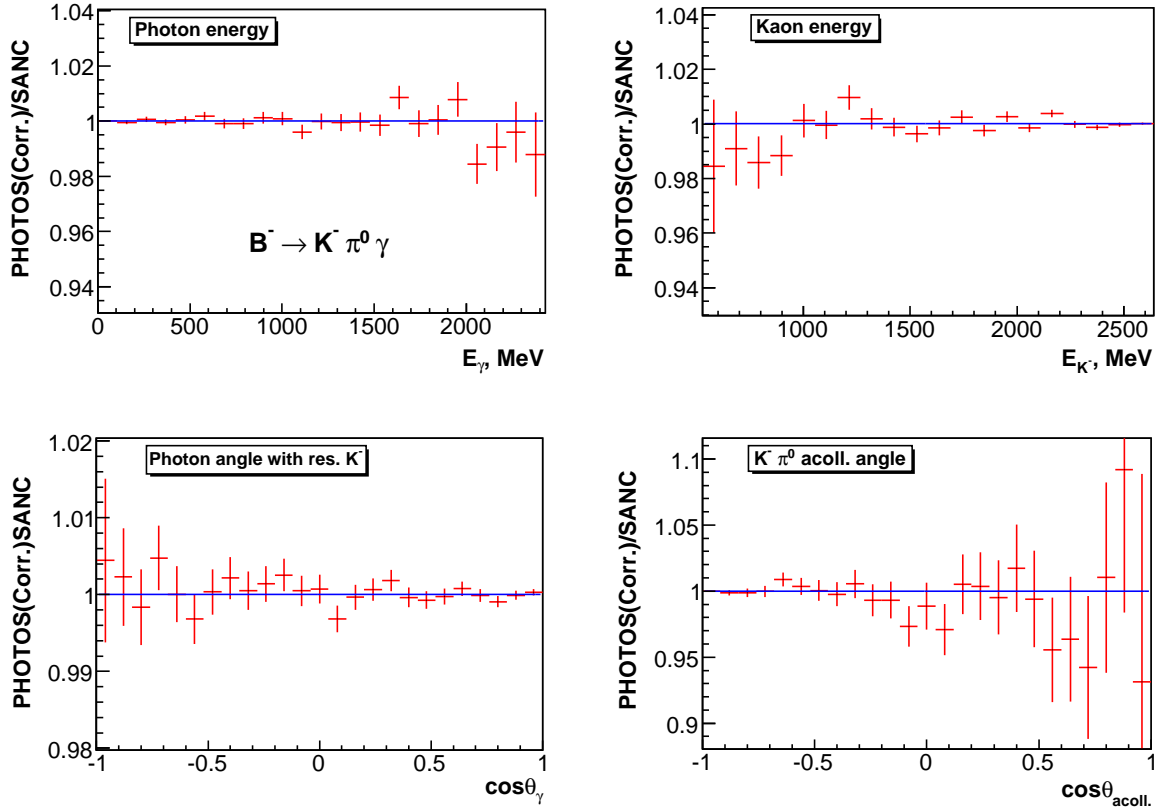


Figure 3: Results from PHOTOS with the exact matrix element, and SANC for ratios of the $B^- \rightarrow \pi^0 K^- (\gamma)$ distributions. Differences between PHOTOS and SANC are below statistical error for samples of 10^9 events.

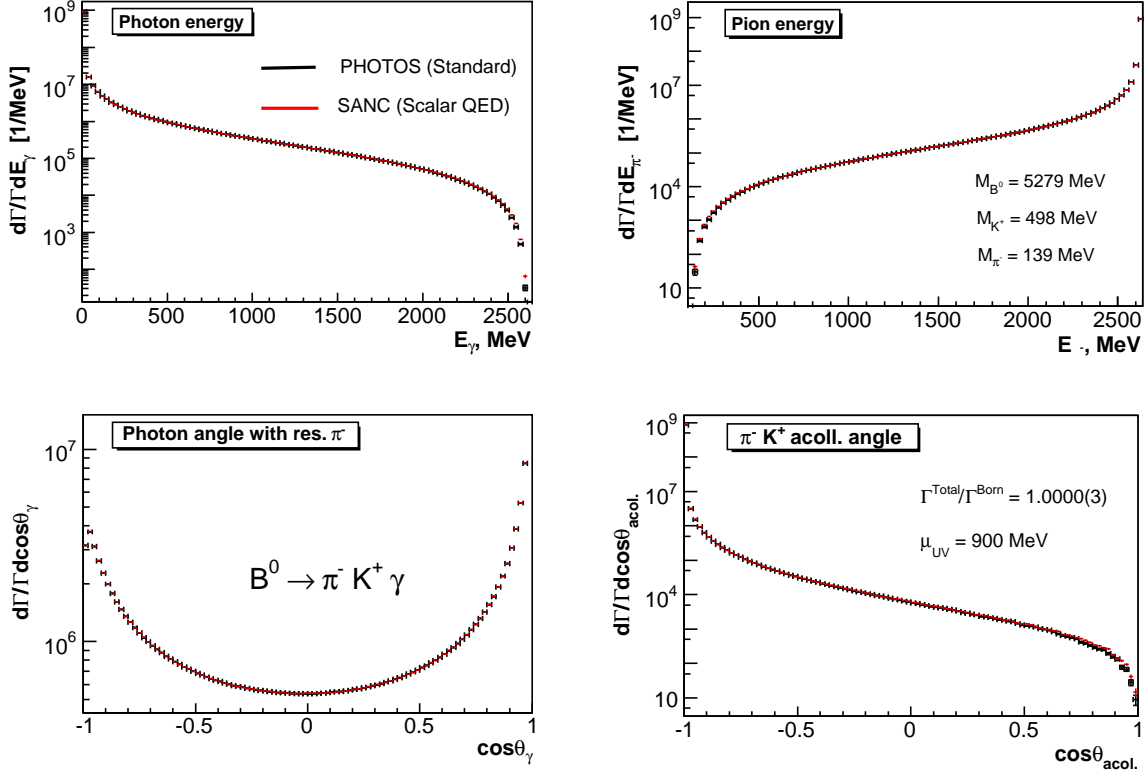


Figure 4: Results from PHOTOS, standard version, and SANC for $B^0 \rightarrow \pi^- K^+ (\gamma)$ decay are superimposed on the consecutive plots. Standard distributions, as defined in the text and logarithmic scales are used. The distributions from the two programs overlap almost completely. Samples of 10^9 events were used. The ultraviolet scale, μ_{UV} , was chosen to leave total decay width unchanged by QED.

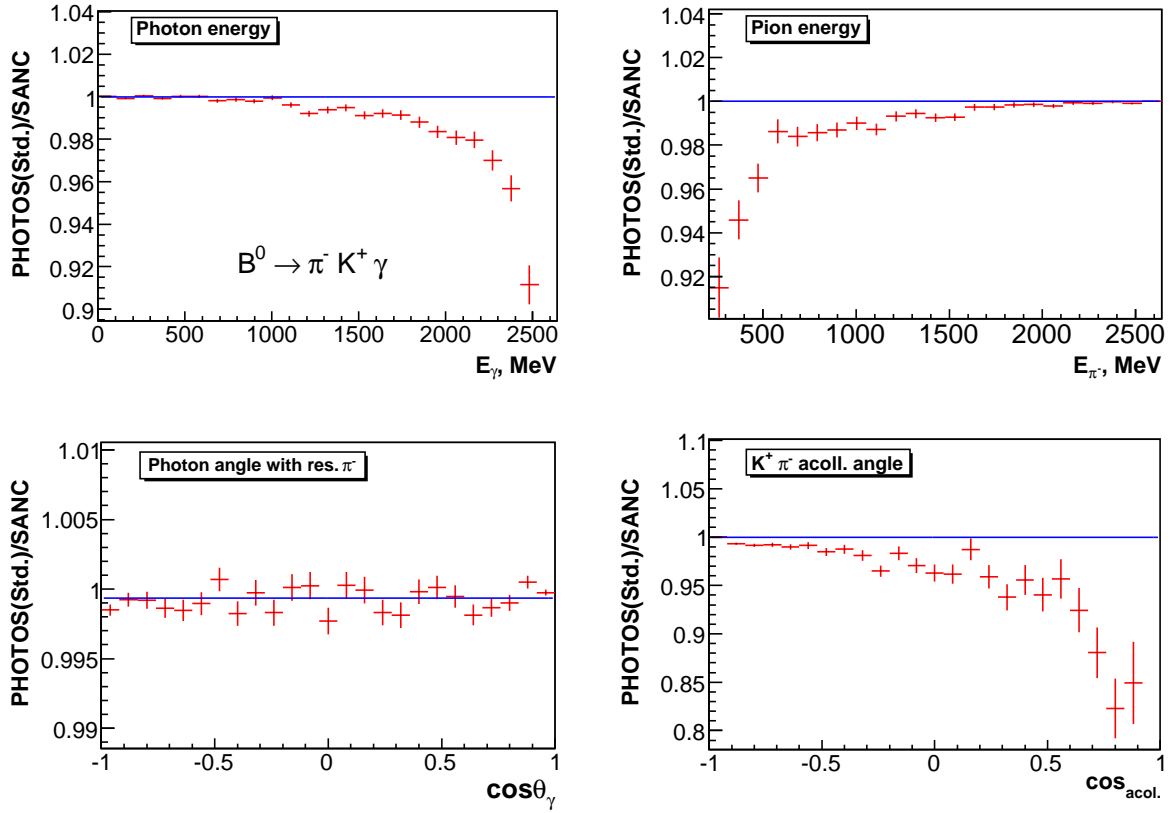


Figure 5: Results from PHOTOS, standard version, and SANC for ratios of the $B^0 \rightarrow \pi^- K^+ (\gamma)$ distributions in fig.4 are presented. Differences between PHOTOS and SANC are small, but are clearly visible now.

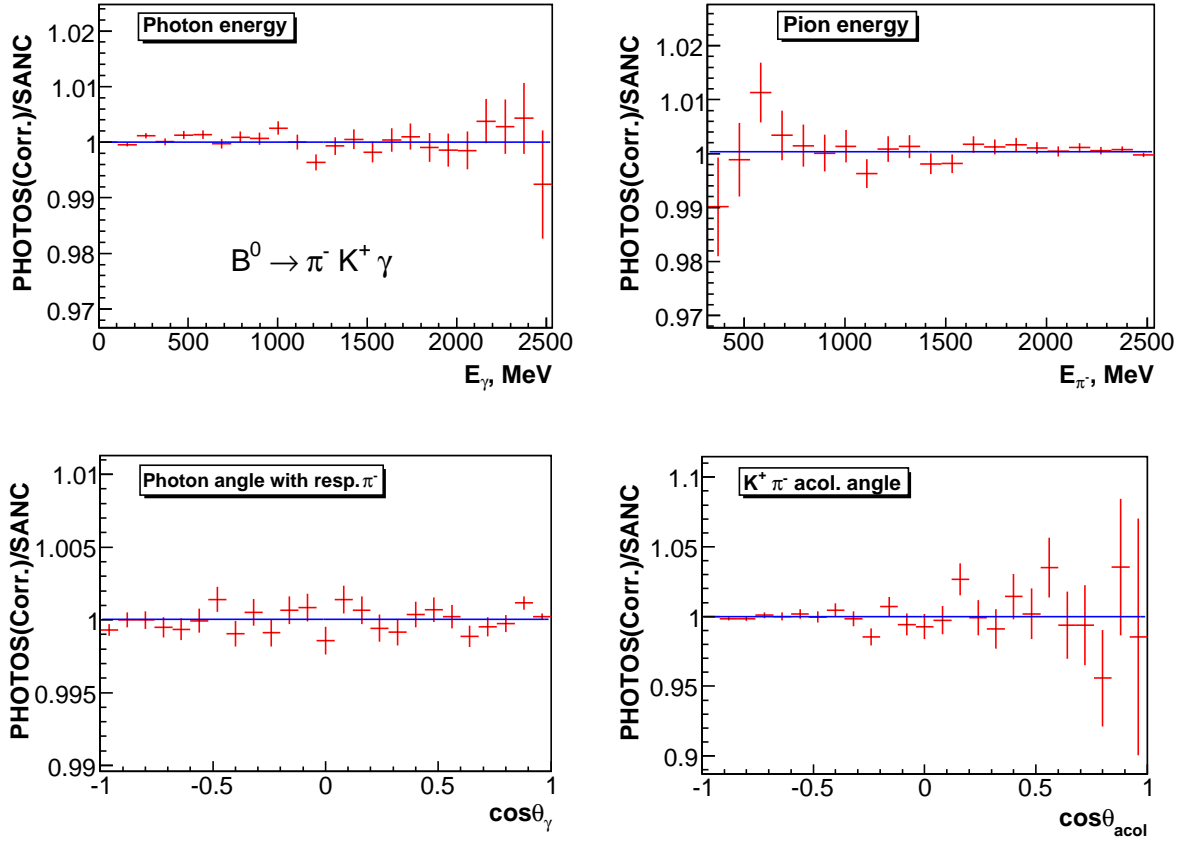


Figure 6: Results from PHOTOS with the exact matrix element, and SANC for ratios of the $B^0 \rightarrow \pi^- K^+ (\gamma)$ distributions. Differences between PHOTOS and SANC are below statistical error for samples of 10^9 events.

Channel	μ_{UV} [MeV]	E_{test} [MeV]	SANC	PHOTOS: $O(\alpha)$	$O(\alpha^2)$	$O(exp)$
$B^- \rightarrow \pi^- \pi^0$	2500	2.6	0.9291	0.9289	0.9314	0.9311
$B^- \rightarrow \pi^- \pi^0$	2500	26	0.9571	0.9569	0.9578	0.9577
$B^- \rightarrow \pi^- K^0$	2500	2.6	0.9294	0.9292	0.9318	0.9314
$B^- \rightarrow \pi^- K^0$	2500	26	0.9574	0.9572	0.9580	0.9580
$B^- \rightarrow K^- \pi^0$	2500	2.6	0.9627	0.9628	0.9636	0.9634
$B^- \rightarrow K^- \pi^0$	2500	26	0.9777	0.9777	0.9779	0.9779
$B^- \rightarrow K^- K^0$	2500	2.6	0.9629	0.9631	0.9639	0.9638
$B^- \rightarrow K^- K^0$	2500	26	0.9779	0.9779	0.9782	0.9781
$B^0 \rightarrow \pi^- \pi^+$	900	2.6	0.8311	0.8306	0.8451	0.8433
$B^0 \rightarrow \pi^- \pi^+$	900	26	0.8978	0.8972	0.9019	0.9016
$B^0 \rightarrow \pi^- K^+$	900	2.6	0.8662	0.8660	0.8754	0.8741
$B^0 \rightarrow \pi^- K^+$	900	26	0.9193	0.9188	0.9219	0.9219
$B^0 \rightarrow K^- \pi^+$	900	2.6	0.8661	0.8659	0.8753	0.8743
$B^0 \rightarrow K^- \pi^+$	900	26	0.9193	0.9191	0.9220	0.9219
$B^0 \rightarrow K^- K^+$	900	2.6	0.9011	0.9014	0.9066	0.9057
$B^0 \rightarrow K^- K^+$	900	26	0.9407	0.9407	0.9424	0.9422

Table 2: Benchmark results for B decays into pair of scalars: electromagnetic cumulative of decay width $\Gamma(E_{test})/\Gamma^{Total}$, where E_{test} denotes the maximal energy which can be carried out by photons. The following input parameters were used: $m_B = 5279$ MeV, $m_{\pi^0} = 135$ MeV, $m_{\pi^\pm} = 139$ MeV, $m_{K^0} = 494$ MeV, $m_{K^\pm} = 498$ MeV. Our results differ negligibly between standard PHOTOS and the one with exact matrix element that is why only one set of numerical results is provided. For each decay channel PHOTOS results of first, second and multiple photon radiation are to a good precision in the following proportion $1 - x : 1 - x + x^2/2 : exp(-x)$, where x for each line of the Table is different; it depends on the decay channel and E_{test} . To produce results for our table samples of 10^7 events were used. Statistical errors are thus at the level of the last significant digit for all the table entries.

Appendix: Details and properties of the explicit phase space parametrization

The formule (17,24) are central in the definition of the PHOTOS algorithm and its phase-space parametrization. For the general description details were not important. In practice, they are nonetheless essential, and all angles masses (or energies) used in formulas (20,21) must be specified. In particular all reference frames used in the definition of angles must be defined.

We will start with the detailed description of parametrizations for two body and three body phase spaces, the latter one with an additional single photon which accompanies the final state of two massive (not necessarily of equal masses) objects. In both cases, the decay of an object

of the mass M and four momentum P is taken into account. The straightforward extension for the parametrization of the multibody decay will be introduced with the help of the footnote, properties will be discussed later in the text.

Our particular choice of the phase-space parametrization is of course motivated by the necessity to regularize the infrared and collinear singularities. On the other hand, the definition itself does not need singularities to be exposed, or even to be present at all. To ease reading, let us point out that (at first) we will expect the collinear singularity to be present only when the photon becomes parallel to the direction of k_1 . Later, we will discuss the case when both final states (of momentum k_1 and k_2) are charged and thus the singularity may appear along the two directions. We will continue with the case when the photon accompanies a multi-particle/multi-charge final state and on the necessity to introduce several simultaneous parametrizations, to be used in Monte Carlo parallel generation *channels*, used at each step of iteration as defined in formula (24).

In the following eight points we define the angles used for the two-body phase-space parametrization, and continue with the definition of phase-space variables of the two-body plus photon case.

1. For the definition of coordinate system in the P -rest frame the \hat{x} and \hat{y} axes of the laboratory frame boosted to the rest frame of P can be used. The orthogonal right-handed system can be constructed with their help in a standard way.
2. We choose polar angles θ_1 and ϕ_1 defining the orientation of the four momentum \bar{k}_2 in the rest frame of P . In that frame \bar{k}_1 and \bar{k}_2 are back to back¹⁴, see fig. (7).
3. The previous two points would complete the definition of the two-body phase space, if both \bar{k}_1 and \bar{k}_2 had no measurable spin degrees of freedom visualizing themselves e.g. through correlations of the secondary decay products' momenta. Otherwise we need to know an additional angle ϕ_X to complete the set of Euler angles defining the relative orientation of the axes of the P rest-frame system with the coordinate system used in the rest-frame of \bar{k}_2 (and possibly also of \bar{k}_1), see fig. (8).
4. If both rest-frames of \bar{k}_1 and \bar{k}_2 are of interest, their coordinate systems are oriented with respect to P with the help of θ_1, ϕ_1, ϕ_X . We assume that the coordinate systems of \bar{k}_1 and \bar{k}_2 are connected by a boost along the \bar{k}_2 direction, and in fact share axes: $z' \uparrow \downarrow z'', x' \uparrow \uparrow x'', y' \uparrow \downarrow y''$.
5. Let us turn now to the three-body phase space parametrization. We take the photon energy k_γ in the rest frame of P , with its help we calculate: photon, k_1 and k_2 energies, all in $k_1 + k_2$ frame.
6. We use the angles θ, ϕ , in the rest-frame of the $k_1 + k_2$ pair: angle θ is an angle between the photon and k_1 direction (i.e. $-z''$). Angle ϕ defines the photon azimuthal angle around z'' , with respect to x'' axis (of the k_2 rest-frame), see fig. (9).

¹⁴In the case of phase space construction for multi-body decays \bar{k}_2 should read as a state representing the sum of all decay products of P but \bar{k}_1 .

7. If all k_1 , k_2 and $k_1 + k_2$ rest-frames exist, then the x -axes for the three frames are chosen to coincide. It is possible, because they are all connected by the boosts along the common z'' direction, see fig. (9). The axes of $k_1 + k_2$ rest-frame are not drawn explicitly.
8. To define orientation of k_2 in P rest-frame coordinate system, and to complete construction of the whole event, we will re-use Euler angles of \bar{k}_2 : ϕ_X , θ_1 and ϕ_1 (see figs. 10 and 11), defined again of course in the rest frame of P .

That completes our definitions of parametrizations for the two-body and three-body phase spaces necessary to define transformation G of formulas (20,21). Before commenting on the properties of our parametrizations, let us note that these parametrizations were already used and defined in ref. [2], in all details, except for the function of (only implicitly introduced there) angle ϕ_X . For some readers, definition from that paper may be also easier to follow.

Let us comment, now, on these properties of our parametrizations which are important for construction of the PHOTOS algorithm.

- a) The parametrizations of the two-body and three-body phase-space (photon included) are used for the explicit kinematical construction denoted by formula (17). We can replace the roles played by k_1 and k_2 . This simple operation leads to a new phase-space parametrization, which can be used in a second branch of the Monte Carlo generation.
- b) The phase-space Jacobians (factor W_n^{n+1} of (17)) are identical for the two branches; this factor is also never larger than $k_\gamma \frac{1}{2(2\pi)^3}$.
- c) Angle θ of the first branch coincides with $\pi - \theta$ of the second one.
- d) In the soft ($k_\gamma \rightarrow 0$) and collinear ($\theta \rightarrow 0$ or π) limits, angles θ_1 , ϕ_1 , ϕ_X of the two branches converge to each other (in these limits they may differ by π or 2π).
- e) Properties (c) and (d) are convenient for our construction of the weights given by formula (30), because they coincide with the similar properties of the exact matrix element.
- f) Thanks to property (b), also the first version of (30) is exact. In fact, this first version is more suitable for multi-photon radiation, if first order matrix element is used only. This observation required comparisons with second order matrix elements [14]. The choice of \bar{k}_2 (or k_2) direction to define θ_1 , ϕ_1 , rather than \bar{k}_1 , was also motivated by the properties of the decay matrix elements.

Let us present now some further observations¹⁵, which go beyond NLO corrections for the processes discussed in ref. [14] and in the present paper, and point to applications for a multi-body/multi-charge final states.

¹⁵ Note, that the approximations to be discussed in the following points, result from matching kinematical branches and affect the way how phase-space Jacobians are used in (30). The full phase space remain covered, as is the case of formule (17,24) denoting exact phase-space parametrization of single and multi-photon final state.

- Property (d) extends to more than two-body decays, and also to cases when there are more than two charged particles present in the final state. The relation between angles θ_1, ϕ_1, ϕ_X of the distinct branches is more complex, but in the discussed limits still independent from θ and ϕ .
- Extended property (d) and property (e) enable the use of (30) for multi-photon radiation; this also holds in the case when more than two charged particles are present in the final state.
- That is why, in the case of two-body decays (plus bremsstrahlung photons), such type of phase-space treatment is sufficient for the NLO precision.
- For the NNLO precision, in matching of the two mappings for the collinear singularities¹⁶ another factor of the type $\lambda^{1/2}(\dots)/\lambda^{1/2}(\dots)$ would have to be included in W_n^{n+1} of formulas (17,30). In fact in such a case the exact multi-photon phase space parametrization would be preserved.
- For each additional charged decay product present in the final state, still another factor of the type $\lambda^{1/2}(\dots)/\lambda^{1/2}(\dots)$ is needed in W_n^{n+1} to assure multichannel generation with the exact treatment of the phase space.
- Even without future refinements (as explained in the previous two points) our phase space parametrization is sufficient for NLO and NLL precision for the two-body (two-charges) decays, accompanied with arbitrary number of photons. In a general case, when more than two charged particles are present in final state, such phase space parametrization remains sufficient for LL only, even though also in this case, the full multi-photon phase space is covered. At present, the resulting precision is sufficient and does not justify those easy changes.
- In our choice of phase space parametrization (point 1), we have dropped some details, the choice of $\hat{x}, \hat{y}, \hat{z}$ axes of the P rest-frame were not specified. Indeed, for the decay of a scalar object, such as that discussed in the present paper, every choice is equivalent. In general, it is not the case. Already in case of the Z boson decay, the choice of the \hat{z} axis parallel to the direction of the incoming beam of the same charge as k_2 is advantageous, see ref. [14] where the process $e^+e^- \rightarrow Z \rightarrow l^+l^-n(\gamma)$ was studied. In this case the direction of the incoming beam coincides with the spin state of Z , and the choice simplify expression for matrix element.
- Finally, we may consider extending our method beyond the decays. In the case of the t -channel processes, or initial state radiation, particular choices for the frames and angles would be also essential for the construction to match the structure of the matrix element singularities. Some hints into that direction can be seen already now, refs. [25, 26].

¹⁶ Such matching is necessary for the two branches of the generation, used to presample collinear singularities along the directions of k_1 and k_2 , to be used simultaneously in construction of each event.

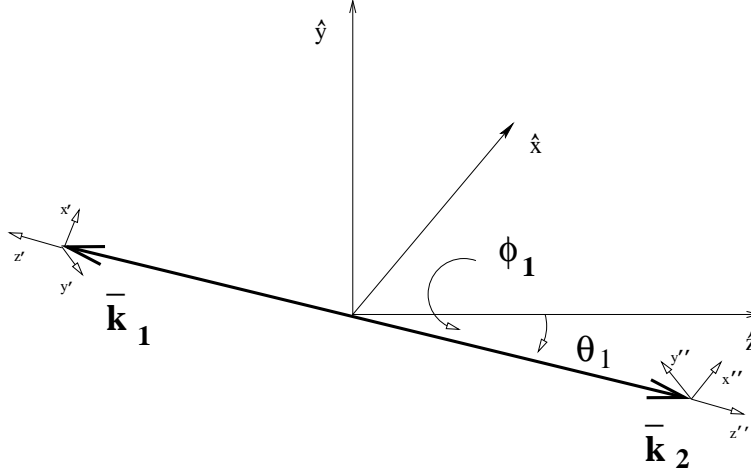


Figure 7: The angles θ_1, ϕ_1 defined in the rest-frame of P and used in parametrization of two-body phase-space.

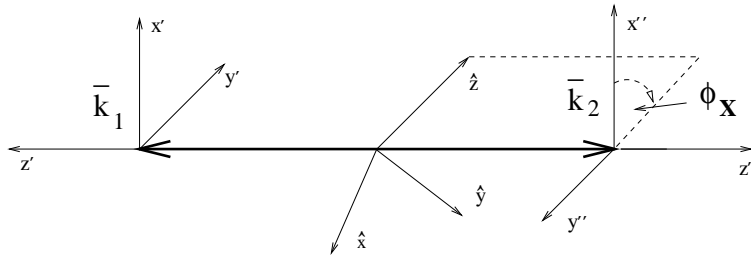


Figure 8: Angle ϕ_X is also defined in the rest-frame of P as an angle between (oriented) planes spanned on: (i) \bar{k}_1 and \hat{z} -axis of the P rest-frame system, and (ii) \bar{k}_1 and x'' -axis of the \bar{k}_2 rest frame. It completes definition of the phase-space variables if internal orientation of \bar{k}_1 system is of interest. In fact, Euler angle ϕ_X is inherited from unspecified in details, parametrization of phase space used to describe possible future decay of \bar{k}_2 (or \bar{k}_1).

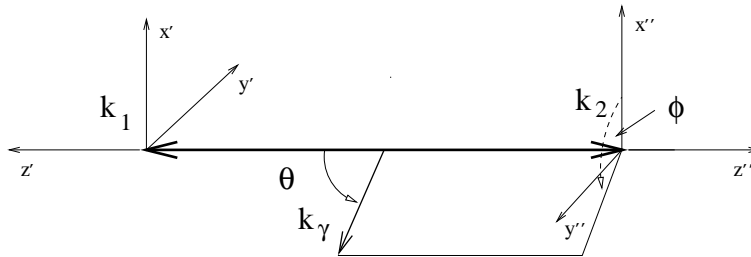


Figure 9: The angles θ, ϕ are used to construct the four-momentum of k_γ in the rest-frame of $k_1 + k_2$ pair (itself not yet oriented with respect to P rest-frame). To calculate energies of k_1, k_2 and photon, it is enough to know m_1, m_2, M and photon energy k_γ of the P rest-frame.

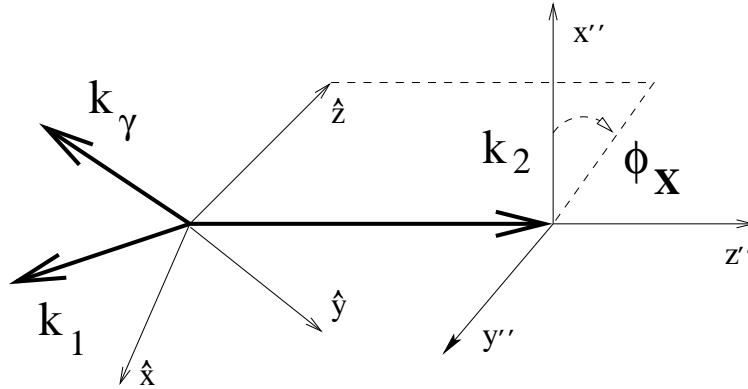


Figure 10: Use of angle ϕ_x in defining orientation of k_1 , k_2 and photon in the rest-frame of P . At this step only the plane spanned on P frame axis \hat{z} and k_2 is oriented with respect to $k_2 \times x''$ plane.

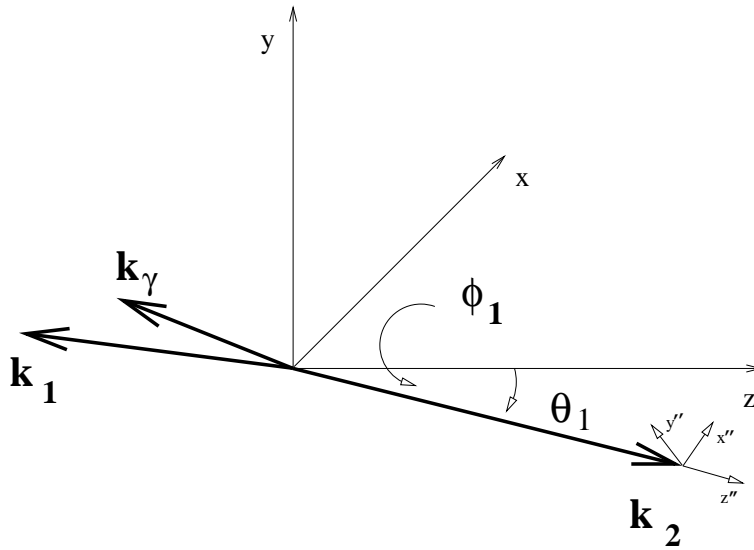


Figure 11: Final step in event construction. Angles θ_1 , ϕ_1 are used. The final orientation of k_2 coincide with this of \bar{k}_2 .

References

- [1] E. Barberio, B. van Eijk, and Z. Was, *Comput. Phys. Commun.* **66** (1991) 115.
- [2] E. Barberio and Z. Was, *Comput. Phys. Commun.* **79** (1994) 291–308.
- [3] M. A. Dobbs *et al.*, hep-ph/0403045.
- [4] CDF Collaboration, V. M. Abazov *et al.*, *Phys. Rev.* **D70** (2004) 092008, hep-ex/0311039.
- [5] OPAL Collaboration, G. Abbiendi *et al.*, *Phys. Lett.* **B580** (2004) 17–36, hep-ex/0309013.
- [6] DELPHI Collaboration, J. Abdallah *et al.*, *Eur. Phys. J.* **C31** (2003) 139–147, hep-ex/0311004.
- [7] NA48 Collaboration, A. Lai *et al.*, *Phys. Lett.* **B602** (2004) 41–51, hep-ex/0410059.
- [8] KTeV Collaboration, T. Alexopoulos *et al.*, *Phys. Rev.* **D71** (2005) 012001, hep-ex/0410070.
- [9] Belle Collaboration, A. Limosani *et al.*, hep-ex/0504046.
- [10] BABAR Collaboration, B. Aubert *et al.*, *Phys. Rev.* **D69** (2004) 111103, hep-ex/0403031.
- [11] FOCUS Collaboration, J. M. Link *et al.*, hep-ex/0412034.
- [12] P. Golonka and Z. Was, hep-ph/0508015.
- [13] P. Golonka and Z. Was, *Eur. Phys. J.* **C45** (2006) 97–107, hep-ph/0506026.
- [14] P. Golonka and Z. Was, hep-ph/0604232, EPJC in print; 10.1140/epjc/s10052-006-0205-3.
- [15] A. Andonov *et al.*, *Comput. Phys. Commun.* **174** (2006) 481–517, hep-ph/0411186.
- [16] F. James, FOWL - a General Monte-Carlo Phase Space Program, 1977, CERN Computer Centre Program Library, Long Writeup W505.
- [17] T. Kinoshita, *J. Math. Phys.* **3** (1962) 650.
- [18] T. D. Lee and M. Nauenberg, *Phys. Rev.* **B133** (1964) 1549.
- [19] E. Baracchini and G. Isidori, *Phys. Lett.* **B633** (2006) 309–313, hep-ph/0508071.
- [20] Z. Was, Written on the basis of lectures given at the 1993 European School of High Energy Physics, Zakopane, Poland, 12-25 Sep 1993, CERN-TH-7154-94.

- [21] S. Jadach, Z. Was, R. Decker and J. H. Kuhn, *Comput. Phys. Commun.* **76** (1993) 361.
- [22] A. Andonov, S. Jadach, G. Nanava, and Z. Was, *Acta Phys. Polon.* **B34** (2003) 2665–2672, hep-ph/0212209.
- [23] G. Nanava and Z. Was, *Acta Phys. Polon.* **B34** (2003) 4561–4570, hep-ph/0303260.
- [24] S. Jadach, B. F. L. Ward and Z. Was, *Phys. Rev. D* **63** (2001) 113009 [arXiv:hep-ph/0006359].
- [25] Z. Was, *Eur. Phys. J. C* **44** (2005) 489 [arXiv:hep-ph/0406045].
- [26] F. A. Berends, R. Kleiss and S. Jadach, *Nucl. Phys.* **B202** (1982) 63.